Critical Energy Dissipation in a Binary Superfluid Gas by a Moving Magnetic Obstacle

Joon Hyun Kim[1], Deokhwa Hong,[1,2] Kyuhwan Lee,[1,2] and Y. Shin[1,2,*]

[1]*Department of Physics and Astronomy, and Institute of Applied Physics, Seoul National University, Seoul 08826, Korea*
[2]*Center for Correlated Electron Systems, Institute for Basic Science, Seoul 08826, Korea*

We study the critical energy dissipation in an atomic superfluid gas with two symmetric spin components by an oscillating magnetic obstacle. Above a certain critical oscillation frequency, spin-wave excitations are generated by the magnetic obstacle, demonstrating the spin superfluid behavior of the system. When the obstacle is strong enough to cause density perturbations via local saturation of spin polarization, half-quantum vortices (HQVs) are created for higher oscillation frequencies, which reveals the characteristic evolution of critical dissipative dynamics from spin-wave emission to HQV shedding. Critical HQV shedding is further investigated using a pulsed linear motion of the obstacle, and we identify two critical velocities to create HQVs with different core magnetization.

Spin superfluidity, the absence of energy dissipation in a spin current, is a fascinating macroscopic quantum phenomenon. It was first observed in liquid ³He [1] and recently investigated in various magnetic materials [2–4], suggesting its potential applications in spintronics [5]. One minimal setting allowing the remarkable phenomenon is a binary superfluid system, which consists of two symmetric superflowing components. Owing to the $\mathbb{Z}_2$ symmetry, the system has two Goldstone modes corresponding to pure phonons and magnons [6], which are associated with mass and spin superfluidity, respectively [7,8]. In cold atom experiments, such a symmetric binary superfluid system was realized with spin-1 antiferromagneteic Bose-Einstein condensates (BECs) of ²³Na. Its spin superfluid behavior was demonstrated by observing the absence of damping in spin dipole oscillations of trapped samples [9,10]. Two sound modes in the mass and spin sectors were also observed [11].

One of the key characteristics of a superfluid is the critical velocity for its frictionless flow against external perturbations. In a conventional scalar superfluid with broken $U(1)$ symmetry, it is known that when it flows past an obstacle, energy dissipation occurs above a certain critical velocity via phonon radiation [12] and nucleation of vortices [13], arising from the local accumulation of superfluid phase slippages [14]. An interesting question about a spin superfluid is how it responds to a moving *magnetic* obstacle, i.e., an obstacle that induces different perturbations to each spin component [15]. Based on the analogy between the mass and spin sectors, it is expected that magnon excitations would be generated above a certain critical velocity. However, the situation is different for vortex nucleation because its fundamental topological excitations are vortices with fractional circulation, which are called half-quantum vortices (HQVs) [16]. A HQV contains both mass and spin circulations, and therefore, its

nucleation cannot be fulfilled by a pure phase slip process in the spin sector.

In this Letter, we investigate the critical dissipative dynamics in a symmetric binary superfluid by an oscillating magnetic obstacle. Pertaining to a weak obstacle, which does not saturate local spin polarization, a sudden onset of spin-wave excitations is observed with increasing the oscillation frequency, which demonstrates the spin superfluidity of the system. Surprisingly, the creation of HQVs is not observed for the weak magnetic obstacle whose speed exceeds the spin sound velocity. On the other hand, with a strong magnetic obstacle, which can produce mass density perturbations by inducing local saturation of spin polarization, HQVs can be created by moving the obstacle above a certain critical velocity. Furthermore, we find that the critical velocities are different for the two types of HQVs with different core magnetizations, which originate from the magnetic property of the obstacle. This study demonstrates spin superfluid behavior of a binary superfluid system against external magnetic perturbations, and furthermore, reveals the evolution of critical dissipative dynamics from spin-wave emission to HQV shedding in a spin superfluid.

Our experiment starts with a BEC of ²³Na in the $|F = 1, m_F = 0\rangle$ hyperfine ground state in an optical dipole trap [9]. The condensate contains about 2.7×10^6 atoms, and its Thomas-Fermi radii are $(R_x, R_y, R_z) \approx (162, 106, 1.5)$ μm for trapping frequencies of $(\omega_x, \omega_y, \omega_z) = 2\pi \times (5.8, 8.9, 641)$ Hz. We prepare an equal mixture of atoms in the two spin states, $|\uparrow\rangle \equiv |m_F = 1\rangle$ and $|\downarrow\rangle \equiv |m_F = -1\rangle$, by applying a $\pi/2$ rf pulse to the initial $|m_F = 0\rangle$ state. The two spin components are miscible [17] and constitute a symmetric binary superfluid. The intercomponent interaction strength $g_{\uparrow\downarrow}$ is comparable

095302-1

to the intracomponent interaction strength g given as $(g - g_{\uparrow\downarrow})/g \approx 7\%$ [18], so the mass and spin sectors of the binary system are energetically well separated. For the peak atomic density at the condensate center, the density and spin healing lengths are $\xi_n \approx 0.5$ μm and $\xi_s \approx 2.5$ μm, respectively, and the speed of spin sound is $c_s = 0.63(4)$ mm/s in the highly oblate condensate [11]. During the experiment, spin-changing collisions are suppressed by a large negative quadratic Zeeman energy via microwave field dressing [19]. The external magnetic field is 50 mG, and its gradient on the xy plane is canceled to be less than 0.1 mG/cm [20].

The schematic of our experiment is shown in Fig. 1(a). A magnetic obstacle is realized using a focused 589-nm near-resonant laser beam with circular polarization, which produces repulsive and attractive Gaussian optical potentials for the two $|\uparrow\rangle$ and $|\downarrow\rangle$ states, respectively, with same peak magnitude V_0 [11]. The beam propagates toward the central region of the condensate along the z axis, and its $1/e^2$ radius is about $7\xi_s$. We adiabatically ramp up the obstacle beam for 300 ms and hold it for 100 ms to stabilize the beam intensity. Then, we sinusoidally oscillate the obstacle by manipulating a piezodriven mirror for 1 s at variable oscillation frequency f. The obstacle position is given by $x(t) = A\cos(2\pi f t)$ with $x = 0$ denoting the sample center. The sweep distance is $2A \approx 37$ μm, over which the atomic column density varies less than 5%. After the stirring process, we ramp down the obstacle beam for 300 ms and take a spin-sensitive phase-contrast image of the sample along the z direction to measure the spatial magnetization distribution [16]. We let the condensate
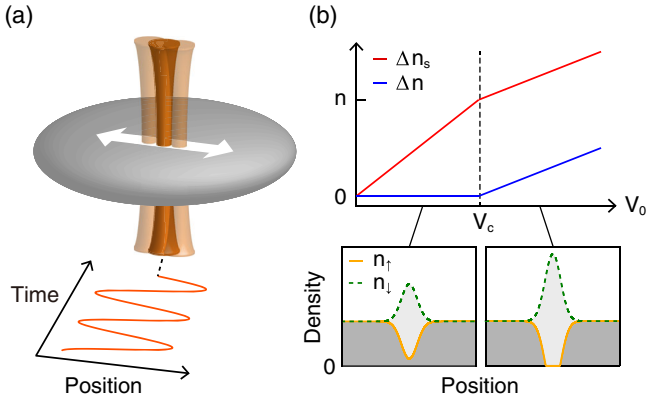

FIG. 1. Oscillating magnetic obstacle in a symmetric binary superfluid. (a) Schematic of the experiment. A focused near-resonant Gaussian laser beam, which provides a repulsive (attractive) potential for the spin-$\uparrow$($\downarrow$) component, undergoes sinusoidal oscillations along a linear path at the central region of the trapped sample. (b) Spin and mass density variations, Δn_s and Δn, as functions of the obstacle strength V_0. For $V_0 > V_c$, the spin polarization is saturated due to the density depletion of the spin-$\uparrow$ component. Insets: the representative density profiles of the spin-$\uparrow$ (yellow solid) and spin-$\downarrow$ (green dashed) components for weak (left) and strong obstacles (right).

expand for 19 ms before applying the imaging light, which facilitates the observation of magnon excitations via their self-interference effect [21], as well as HQVs with their expanded ferromagnetic cores [16].

Perturbations generated by the magnetic obstacle depend on the obstacle strength V_0. Figure 1(b) shows the spin and mass density variations, Δn_s and Δn, induced at the center of a stationary obstacle as a function of V_0, where $\Delta n_s \equiv n_\downarrow - n_\uparrow$ and $\Delta n \equiv n_\downarrow + n_\uparrow - n$ with $n_{\uparrow(\downarrow)}$ being the density of the spin-$\uparrow$($\downarrow$) component and n being the total density without the obstacle. When V_0 is small, the density profiles of the two spin components vary antisymmetrically, yielding $\Delta n_s = 2V_0/(g - g_{\uparrow\downarrow})$ with $\Delta n = 0$, i.e., only spin perturbations are generated by the magnetic obstacle. However, when V_0 is increased over a certain critical strength V_c, the spin-$\uparrow$ component is locally depleted, resulting in $\Delta n > 0$, and thus, mass perturbations are also induced by the magnetic obstacle. The critical strength is given by $V_c = (g - g_{\uparrow\downarrow})n/2$ from $\Delta n_s = n$ and in our experiment, $V_c/\mu \approx 3.5\%$ with $\mu = (g + g_{\uparrow\downarrow})n/2$ being the chemical potential of the condensate. In the following, we call a magnetic obstacle with $V_0/V_c < 1$ (>1) weak (strong).

In Fig. 2, we display a series of magnetization images of the perturbed condensate for various stirring frequencies f with weak and strong magnetic obstacles of $V_0/V_c \approx 0.9$ and 2.2, respectively. As f increases, spin fluctuations in the condensate are observed to be enhanced, indicating that energy dissipation occurs by the oscillating magnetic obstacle. In the case of a strong obstacle, it is noticeable that fully spin-polarized, pointlike domains appear in the condensate at high $f > 3$ Hz [Figs. 2(g) and 2(h)]. This implies that HQVs are generated by the fast moving obstacle, and it is confirmed by taking an image of the sample after Stern-Gerlach spin separation and observing the appearance of density-depleted holes in each spin component [Figs. 2(k) and 2(l)]. By contrast, we observe that HQVs are not created with the weak obstacle for the full range of f in our experiment, where the obstacle's speed reaches over $3c_s$. This suggests that HQV nucleation requires both spin and mass currents, which is consistent with the spin-mass composite nature of the HQVs. HQVs can be indirectly generated via dissociation of spin vortices that have pure spin circulation [16,22], but the spin vortices are energetically too costly because of their density-depleted cores.

To quantitatively characterize the energy dissipation by the oscillating magnetic obstacle, we measure the spatial variance of magnetization, σ_M, at the central region of the condensate. Figure 3 displays the growth of σ_M as a function of the stirring frequency f. For the weak obstacle, we observe a sudden increase of σ_M above a certain critical frequency of $f_c \approx 6$ Hz [23]. This onset behavior indicates the critical generation of spin waves, or magnon excitations, and demonstrates the spin superfluidity of the binary system against external magnetic perturbations. The critical
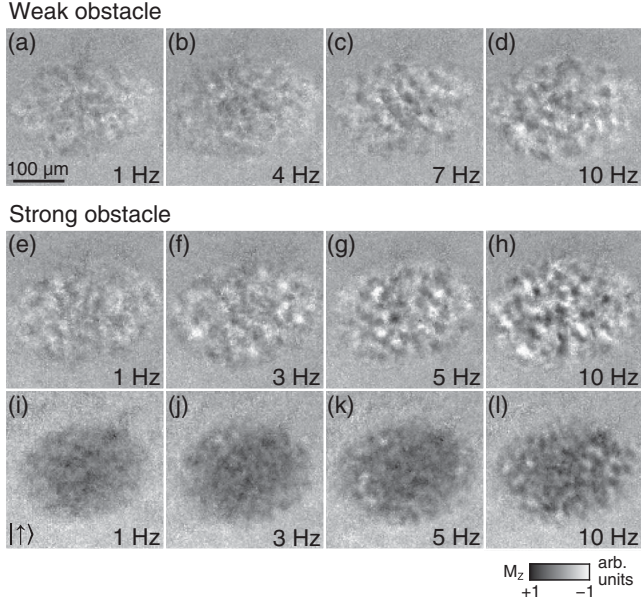
FIG. 2. Generation of spin excitations in a spinor BEC by an oscillating magnetic obstacle. Magnetization (M_z) images of the condensate stirred with an obstacle of $V_0/V_c \approx 0.9$ [(a)–(d)] and ≈ 2.2 [(e)–(h)] for various oscillation frequencies f. The images were obtained after a 19-ms time of flight. Fully magnetized pointlike domains in (g) and (h) indicate HQVs with ferromagnetic cores. (i)–(l) Images of the spin–$\uparrow$ component for the same stirring conditions in (e)–(h), taken after Stern-Gerlach spin separation. The HQVs are distinguishable as density-depleted holes in (k) and (l).

FIG. 3. Critical energy dissipation in the binary superfluid. Magnetization variance σ_M as a function of the oscillation frequency f for the weak (red circles) and strong (blue squares) obstacles. At the top axis, $v_{\max}$ denotes the maximum speed of the oscillating obstacle. σ_M was measured from the area of 157×106 μm^2 at the central region of the condensate. Each data point is the mean value of five to seven measurements of the same experiment, and its error bar represents their standard deviation. Inset: an expanded view on the boxed region at low f.

velocity is measured to be $v_c = 2\pi A f_c \approx 0.7$ mm/s, which is close to the speed of spin sound c_s. As f further increases, σ_M is observed to be saturated and eventually decrease above $f = 16$ Hz. We checked that the stirring time, 1 s, remains in the linear regime with respect to the growth of σ_M [24]. In Refs. [26–28], it was discussed that the excitations are suppressed for a supersonic obstacle due to its finite size.

For the strong obstacle, we observe that σ_M starts growing slowly from a low $f > 1$ Hz (Fig. 3, inset) and shows a rapid jump at $f_{c,v} \approx 4$ Hz. The preceding growth of σ_M indicates the generation of spin waves, while the later rapid increase is due to the HQV shedding, where the magnitude of σ_M is significantly enhanced owing to the fully magnetized vortex cores. The two-step growth of σ_M reveals that the critical dissipative dynamics evolves from spin-wave emission to HQV shedding in the binary superfluid under the perturbations of the strong magnetic obstacle. The critical velocity for the HQV shedding is measured to be $v_{c,v} \approx 0.4$ mm/s, lower than c_s. As f increases over 10 Hz, σ_M gradually decreases. At the extreme case of $f = 50$ Hz, $\sigma_M \approx 0.04$, implying that the generation of HQVs is suppressed.

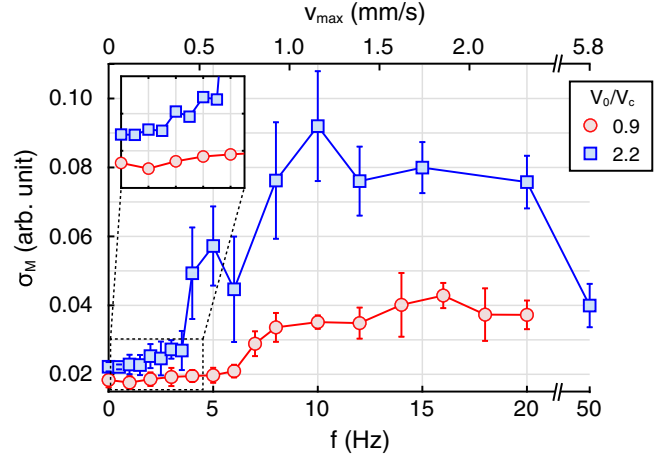The hierarchy between wave and vortex generations by an oscillating obstacle can be understood from the energy accumulation process for vortex nucleation [29,30]. When a drag force arises above the critical velocity v_c, it gradually accumulates energy in the form of local currents and density compression around the moving obstacle [31,32]. In the case of oscillating motion, if the amount of the energy accumulated over the oscillation period falls short of the energy cost of a vortex dipole, it is likely to dissipate through wave emission. It was also theoretically shown that the accelerated motion can stimulate the radiation of waves [29,33]. Here we note that the relation between phonon emission and vortex shedding was not elucidated in previous stirring experiments with atomic superfluid gases, although the critical velocities were identified by observing a sudden increase of sample temperature [34–36], the onset of a pressure gradient [37], and the critical vortex shedding [38–40]. In our experiment, spin-wave excitations as well as HQVs are directly detected using the magnetization imaging in the effective 2D sample ($\xi_s > R_z$), which allows one to decipher the two-step evolution of the critical dissipative dynamics.

There are two types of HQVs according to the core magnetization, and it is an intriguing query which one is more favorable to be nucleated for the given magnetic obstacle. To examine the detailed aspects of the critical HQV shedding, we perform a modified experiment, where the strong obstacle with $V_0/V_c \approx 2.2$ is translated at the central region of the condensate by a fixed distance ≈ 57 μm with a constant velocity v to shed a few pairs of vortices. In Fig. 4(a), representative magnetization images of the condensate after the linear sweep of the obstacle are shown for various velocities v. As v increases,
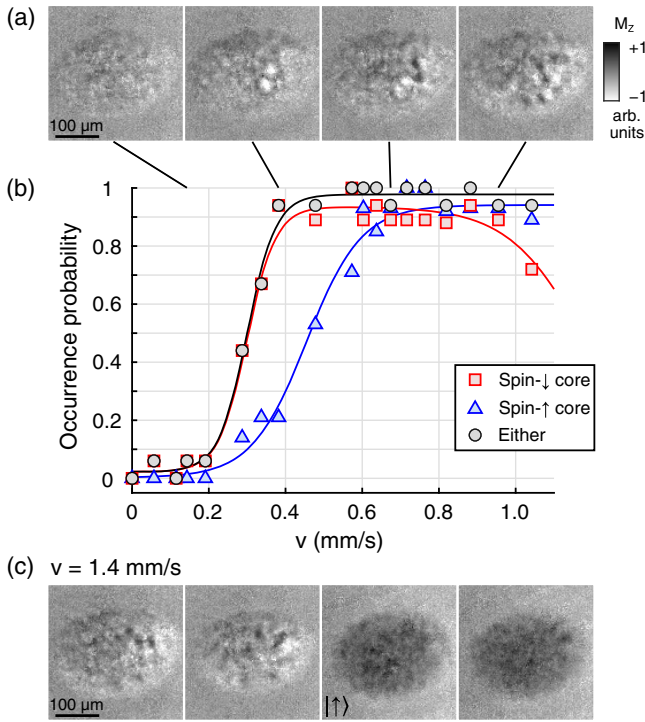
(a)

(b)

(c) v = 1.4 mm/s

FIG. 4.   Critical HQV shedding. (a) Magnetization images of the condensate after a linear sweep of the strong obstacle for various obstacles' moving velocity v. (b) Occurrence probabilities for spin–↓-core HQV (red squares), spin–↑-core HQV (blue triangles), and either of them (black circles) as functions of v. The probabilities for each v were obtained from 14 to 18 measurements of the same experiment. The solid lines denote a guide for the eyes to each data set based on the sigmoid functions. (c) Examples of the magnetization images for $v = 1.4$ mm/s. Only spin–↑-core HQVs appear. The two images on the right side are the images of the spin–↑ component for the same stirring condition.

we observe that the HQV shedding dynamics develops in four stages: (i) no excitation arises in the sample, (ii) a HQV dipole with spin–↓ core begins to shed above a critical velocity, (iii) a HQV dipole with spin–↑ core is also created, and (iv) many HQVs of both types are irregularly generated. The first-shed HQV dipole has cores of the same magnetization as the spin polarization induced by the obstacle.

The occurrence probability $P_{\uparrow(\downarrow)}$ of the HQVs with spin–↑(↓) core is plotted in Fig. 4(b) as a function of v. The onset of vortex generation occurs with the spin–↓-core HQVs at $v \approx 0.3$ mm/s, which is slightly smaller than the measured $v_{c,v}$ in Fig. 3, probably due to the difference of the obstacle's motion. We find that HQVs with spin–↓ core are always present when spin–↑-core HQVs appear at $v \leq 0.4$ mm/s, which implies that the shedding of spin–↑-core HQVs requires higher v, and that $P_\uparrow$ increases more slowly than $P_\downarrow$. In the supersonic regime, $v > 0.6$ mm/s, the correlation between the two HQV sheddings is weakened, and interestingly, $P_\downarrow$ begins to be suppressed prior to $P_\uparrow$. At high $v > 1$ mm/s, it was often observed that

only the spin–↑-core HQVs appeared in the condensate [Fig. 4(c)].

The nucleation of spin–↑-core HQVs is notable because the circulation is formed by the spin component which experiences an attractive potential from the magnetic obstacle. The quantum vortex shedding by an attractive obstacle was not observed in previous experiments [35,36], and the role of the attractive stirrer is still debatable in numerical studies [33,41]. To clarify the issue, we carried out the oscillating obstacle experiment with a scalar condensate containing only the spin–↓ component, where $V_0/\mu \approx 1.7$ and the optical obstacle acts as an attractive one. We observed that vortices are generated by the oscillating attractive obstacle above a certain critical frequency [24]. The same experiment was also performed with a condensate of the spin–↑ component, and it was found that the critical velocity of the attractive obstacle is higher than that of the repulsive one with the same potential magnitude V_0. This observation seems to be accounted for by the local Landau criterion at the obstacle position [29] and provides a qualitative explanation of the measured critical velocities in Fig. 4. Nevertheless, it is important to note that the HQV shedding dynamics cannot be fully described as the sum of the two independent vortex shedding processes. For example, no HQVs were created by the weak obstacle, whereas a penetrable moving obstacle can generate a vortex dipole in a single-component condensate [30]. Note that HQVs have short-range interactions for different core magnetizations, and they are also dynamically coupled to magnons [42].

In conclusion, we have studied the critical dissipative dynamics in an antiferromagnetic spinor BEC by moving a magnetic obstacle. The onset of spin-wave excitations was observed for the weak obstacle, directly probing the spin superfluidity of the binary superfluid. The critical HQV shedding was demonstrated with the strong obstacle, and the two-step evolution of the critical dissipative dynamics provided insight on the hierarchy between wave emission and vortex generation in the superfluid. An interesting extension of this work is to investigate the spinor superfluid near the quantum critical point with zero quadratic Zeeman energy. Spin superfluidity was predicted to vanish due to the full recovery of spin rotation symmetry [9], and novel topological objects such as merons and skrymions may exist stably [43,44].

*yishin@snu.ac.kr
[1] A. S. Borovik-Romanov, Yu. M. Bunkov, V. V. Dmitriev, and Yu. M. Mukharskiy, Observation of phase slippage

during the flow of a superfluid spin current in ^{3}He-B, JETP Lett. **45**, 124 (1987).

[2] D. A. Bozhko, A. A. Serga, P. Clausen, V. I. Vasyuchka, F. Heussner, G. A. Melkov, A. Pomyalov, V. S. L'vov, and B. Hillebrands, Supercurrent in a room-temperature Bose-Einstein magnon condensate, Nat. Phys. **12**, 1057 (2016).

[3] W. Yuan, Q. Zhu, T. Su, Y. Yao, W. Xing, Y. Chen, Y. Ma, X. Lin, J. Shi, R. Shindou, X. C. Xie, and W. Han, Experimental signatures of spin superfluid ground state in canted antiferromagnet Cr_2O_3 via nonlocal spin transport, Sci. Adv. **4**, eaat1098 (2018).

[4] P. Stepanov, S. Che, D. Shcherbakov, J. Yang, R. Chen, K. Thilahar, G. Voigt, M. W. Bockrath, D. Smirnov, K. Watanabe, T. Taniguchi, R. K. Lake, Y. Barlas, A. H. MacDonald, and C. N. Lau, Long-distance spin transport through a graphene quantum Hall antiferromagnet, Nat. Phys. **14**, 907 (2018).

[5] V. Baltz, A. Manchon, M. Tsoi, T. Moriyama, T. Ono, and Y. Tserkovnyak, Antiferromagnetic spintronics, Rev. Mod. Phys. **90**, 015005 (2018).

[6] Y. Kawaguchi and M. Ueda, Spinor Bose-Einstein condensates, Phys. Rep. **520**, 253 (2012).

[7] E. B. Sonin, Spin currents and spin superfluidity, Adv. Phys. **59**, 181 (2010).

[8] J. Armaitis and R. A. Duine, Superfluidity and spin superfluidity in spinor Bose gases, Phys. Rev. A **95**, 053607 (2017).

[9] J. H. Kim, S. W. Seo, and Y. Shin, Critical Spin Superflow in a Spinor Bose-Einstein Condensate, Phys. Rev. Lett. **119**, 185302 (2017).

[10] E. Fava, T. Bienaimé, C. Mordini, G. Colzi, C. Qu, S. Stringari, G. Lamporesi, and G. Ferrari, Observation of Spin Superfluidity in a Bose Gas Mixture, Phys. Rev. Lett. **120**, 170401 (2018).

[11] J. H. Kim, D. Hong, and Y. Shin, Observation of two sound modes in a binary superfluid gas, Phys. Rev. A **101**, 061601 (R) (2020).

[12] G. E. Astrakharchik and L. P. Pitaevskii, Motion of a heavy impurity through a Bose-Einstein condensate, Phys. Rev. A **70**, 013608 (2004).

[13] E. Varoquaux, Anderson's consideration on the flow of superfluid helium: Some offshoots, Rev. Mod. Phys. **87**, 803 (2015).

[14] B. Jackson, J. F. McCann, and C. S. Adams, Vortex Formation in Dilute Inhomogeneous Bose-Einstein Condensate, Phys. Rev. Lett. **80**, 3903 (1998).

[15] J. H. Jung, H. J. Kim, and Y. Shin, Spin and mass currents near a moving magnetic obstacle in a two-component Bose-Einstein condensate, J. Korean Phys. Soc. **78**, 19 (2021).

[16] S. W. Seo, S. Kang, W. J. Kwon, and Y. Shin, Half-Quantum Vortices in an Antiferromagnetic Spinor Bose-Einstein Condensate, Phys. Rev. Lett. **115**, 015301 (2015).

[17] J. Stenger, S. Inouye, D. M. Stamper-Kurn, H.-J. Miesner, A. P. Chikkatur, and W. Ketterle, Spin domains in ground-state Bose-Einstein condensates, Nature (London) **396**, 345 (1998).

[18] S. Knoop, T. Schuster, R. Scelle, A. Trautmann, J. Appmeier, M. K. Oberthaler, E. Tiesinga, and E. Tiemann, Feshbach spectroscopy and analysis of the interaction potentials of ultracold sodium, Phys. Rev. A **83**, 042704 (2011).

[19] F. Gerbier, A. Widera, S. Főlling, O. Mandel, and I. Bloch, Resonant control of spin dynamics in ultracold quantum gases by microwave dressing, Phys. Rev. A **73**, 041602(R) (2006).

[20] J. H. Kim, D. H. Hong, S. Kang, and Y. Shin, Metastable hard-axis polar state of a spinor Bose-Einstein condensate under a magnetic field gradient, Phys. Rev. A **99**, 023606 (2019).

[21] S. W. Seo, J. Choi, and Y. Shin, Scaling behavior of density fluctuations in an expanding quasi-two-dimensional degenerate Bose gas, Phys. Rev. A **89**, 043606 (2014).

[22] F. Manni, K. G. Lagoudakis, T. C. H. Liew, R. Andr, V. Savona, and B. Deveaud, Dissociation dynamics of singly charged vortices into half-quantum vortex pairs, Nat. Commun. **3**, 1309 (2012).

[23] f_c is much higher than the spin dipole oscillation frequency of the trapped sample, which is given by $\approx 0.21\omega_x = 2\pi \times 1.2$ Hz [10].

[24] See Supplemental Material at http://link.aps.org/supplemental/10.1103/PhysRevLett.127.095302 for further details on the magnetic obstacle, the stirring time dependence of σ_M, and vortex generation by an attractive obstacle, which includes Ref. [25].

[25] R. Grimm, M. Weidemüller, and Y. B. Ovchinnikov, Optical dipole traps for neutral atoms, Adv. At. Mol. Opt. Phys. **42**, 95 (2000).

[26] A. Radouani, Soliton and phonon production by an oscillating obstacle in a quasi-one-dimensional trapped repulsive Bose-Einstein condensate, Phys. Rev. A **70**, 013602 (2004).

[27] P. Engels and C. Atherton, Stationary and Nonstationary Fluid Flow of a Bose-Einstein Condensate Through a Penetrable Barrier, Phys. Rev. Lett. **99**, 160405 (2007).

[28] F. Pinsker, Gaussian impurity moving through a Bose-Einstein superfluid, J. Phys. B **521**, 36 (2017).

[29] B. Jackson, J. F. McCann, and C. S. Adams, Dissipation and vortex creation in Bose-Einstein condensed gases, Phys. Rev. A **61**, 051603(R) (2000).

[30] W. J. Kwon, S. W. Seo, and Y. Shin, Periodic shedding of vortex dipoles from a moving penetrable obstacle in a Bose-Einstein condensate, Phys. Rev. A **92**, 033613 (2015).

[31] T. Frisch, Y. Pomeau, and S. Rica, Transition to Dissipation in a Model of Superflow, Phys. Rev. Lett. **69**, 1644 (1992).

[32] T. Winiecki, J. F. McCann, and C. S. Adams, Pressure Drag in Linear and Nonlinear Quantum Fluids, Phys. Rev. Lett. **82**, 5186 (1999).

[33] V. P. Singh, W. Weimer, K. Morgener, J. Siegl, K. Hueck, N. Luick, H. Moritz, and L. Mathey, Probing superfluidity of Bose-Einstein condensates via laser stirring, Phys. Rev. A **93**, 023634 (2016).

[34] C. Raman, M. Köhl, R. Onofrio, D. S. Durfee, C. E. Kuklewicz, Z. Hadzibabic, and W. Ketterle, Evidence for a Critical Velocity in a Bose-Einstein Condensed Gas, Phys. Rev. Lett. **83**, 2502 (1999).

[35] R. Desbuquois, L. Chomaz, T. Yefsah, J. Leonard, J. Beugnon, C. Weitenberg, and J. Dalibard, Superfluid behaviour of a two-dimensional Bose gas, Nat. Phys. **8**, 645 (2012).

[36] W. Weimer, K. Morgener, V. P. Singh, J. Siegl, K. Hueck, N. Luick, L. Mathey, and H. Moritz, Critical Velocity in the BEC-BCS Crossover, Phys. Rev. Lett. **114**, 095301 (2015).

[37] R. Onofrio, C. Raman, J. M. Vogels, J. R. Abo-Shaeer, A. P. Chikkatur, and W. Ketterle, Observation of Superfluid Flow in a Bose-Einstein Condensed Gas, Phys. Rev. Lett. **85,** 2228 (2000).

[38] T. W. Neely, E. C. Samson, A. S. Bradley, M. J. Davis, and B. P. Anderson, Observation of Vortex Dipoles in an Oblate Bose-Einstein Condensate, Phys. Rev. Lett. **104,** 160401 (2010).

[39] W. J. Kwon, G. Moon, S. W. Seo, and Y. Shin, Critical velocity for vortex shedding in a Bose-Einstein condensate, Phys. Rev. A **91,** 053615 (2015).

[40] J. W. Park, B. Ko, and Y. Shin, Critical Vortex Shedding in a Strongly Interacting Fermionic Superfluid, Phys. Rev. Lett. **121,** 225301 (2018).

[41] T. Aioi, T. Kadokura, T. Kishimoto, and H. Saito, Controlled Generation and Manipulation of Vortex Dipoles in a Bose-Einstein Condensate, Phys. Rev. X **1,** 021003 (2011).

[42] S. W. Seo, W. J. Kwon, S. Kang, and Y. Shin, Collisional Dynamics of Half-Quantum Vortices in a Spinor Bose-Einstein Condensate, Phys. Rev. Lett. **116,** 185301 (2016).

[43] J. Choi, W. J. Kwon, and Y. Shin, Observation of Topologically Stable 2D Skyrmions in an Antiferromagnetic Spinor Bose-Einstein Condensate, Phys. Rev. Lett. **108,** 035301 (2012).

[44] A. P. C. Underwood, D. Baillie, P. B. Blakie, and H. Takeuchi, Properties of a nematic spin vortex in an antiferromagnetic spin-1 Bose-Einstein condensate, Phys. Rev. A **102,** 023326 (2020).